Nanoribbons

DOI: 10.1002/anie.201209597

High-Quality Boron Nitride Nanoribbons: Unzipping during Nanotube Synthesis**

Ling Li, Lu Hua Li, Ying Chen,* Xiujuan J. Dai, Peter R. Lamb, Bing-Ming Cheng, Meng-Yeh Lin, and Xiaowei Liu*

Boron nitride nanoribbons (BNNRs) are strips of thin BN sheets with widths on the nanometer scale. BNNRs have unique edge states and width-related properties. First-principle calculations reveal that the bandgaps of zigzag BNNRs relate to nanoribbon width[1] and are tunable by external electric fields and different levels of edge hydrogenation.[1,2] Though bulk hexagonal boron nitride (hBN) crystals are electrically insulating, BNNRs can be made half-metallic through edge hydrogenation, fluorination, and oxygen functionalization.[2,3] Intriguing edge magnetism has also been proposed in BNNRs.[3b,4] An experimental study has shown that BNNRs are much more electrically conductive than boron nitride nanotubes (BNNTs).[5] BNNRs are chemically more reactive than bulk BN owing to the high number of unsaturated edge atoms, which makes them ideal gas-sensing materials. Compared to BN nanotubes and nanosheets, BNNRs could be better composite fillers for improved mechanical enhancement because of stronger interface bindings between BNNR edges and matrix. Therefore, BNNRs are of great interest for nanoscale electronic, spintronic, optoelectronic, sensor, and composite applications. All of these applications require BNNRs in large amounts and high quality. However, the synthesis of nanoribbons is quite challenging. BNNRs have been produced by unzipping BNNTs by postsynthesis treatment, that is, plasma etching and alkali metal intercalation,[5,6] similar to the methods proposed for the production of graphene nanoribbons (GNRs).[7] However, the yield of the current BNNR production is low.

Here, we introduce an in situ unzipping concept for the large-scale production of high-quality nanoribbons. Specifically, BNNTs are longitudinally unzipped during the nanotube synthesis process so that BNNRs are produced directly without the need for postsynthesis treatment. The BNNRs have good crystallinity, high chemical purity, and few point defects in the form of oxygen (O)-decorated nitrogen (N) vacancies, as revealed by near-edge X-ray absorption fine structure (NEXAFS) spectroscopy. The excitonic effects observed from the BNNRs are stronger than those from BNNTs. This in situ unzipping method provides an easy and effective production route to the high-quality BNNRs required for both fundamental research and industrial applications.

To directly produce BNNRs, amorphous boron (B) powder was first ball-milled in anhydrous ammonia gas. The milled B powder was mixed with lithium oxide (Li_2O) powder at Li_2O/B molar ratios of 0.15:1 to 0.30:1. The mixed powder was placed at the bottom of an alumina crucible and heated at 1200 °C in NH_3 gas for 3 h. After heating, a white fluffy product was formed in the crucible. The scanning electron microscopy (SEM) image in Figure 1 a shows that the product contains a high density of needlelike material. The X-ray diffraction (XRD) pattern of the product (Figure 1 b) shows a dominant hBN phase, along with a small amount of rhombohedral boron nitride (rBN) and steel. The existence of the rBN phase is not unusual, since it has been found in BNNTs produced by various methods.[8] The interlayer distance calculated from the (002) diffraction peak is 3.34 Å, typical for hBN and rBN. The steel comes from the collisions between the steel balls and the vial during the ball-milling process.[9] No lithium-related compound is detected in the XRD. Further analyses using X-ray photoelectron spectroscopy (XPS) also confirm the absence of Li in the product (see Figure S1 in the Supporting Information).

A mixture of BNNRs and BNNTs with an unzipping ratio of more than 40 % (72 out of 168) is found in the product during transmission electron microscopy (TEM) investigations. The yield of the BNNRs can be improved to roughly 60 % after a simple purification treatment involving sonication and centrifugation (see the Supporting Information).[10] Figure 2 a shows a partially unzipped BNNR with a length exceeding 2.6 μm and an unzipping stop site at the left (marked with an arrow). Because BNNRs are much more flexible than BNNTs, twists and deformations can be easily observed (see Figure S4 in the Supporting Information).

[*] L. Li, Dr. L. H. Li, Prof. Y. Chen, Dr. X. J. Dai, Dr. P. R. Lamb
Institute for Frontier Materials, Deakin University
Geelong Waurn Ponds Campus, VIC 3216 (Australia)
E-mail: luhua.li@deakin.edu.au
ian.chen@deakin.edu.au
L. Li, Prof. X. Liu
MEMS Center, Harbin Institute of Technology
Harbin 150001 (China)
and Key Laboratory of Micro-systems and Micro-structures Manufacturing, Ministry of Education, Harbin 150001 (China)
Dr. B.-M. Cheng, M.-Y. Lin
National Synchrotron Radiation Research Center
101 Hsin Ann Road, Hsinchu Science Park, Hsinchu 30076 (Taiwan)

[**] L.H.L. thanks W. Kenji and T. Taniguchi from NIMS Japan for providing hBN single crystals, B. Cowie from the Australian Synchrotron for assistance during NEXAFS measurements, H. Zhang and Y. Chen from Trinity College Dublin, Ireland, as well as P. Cizek from Deakin University for help with TEM investigations. We acknowledge the scientific and technical assistance from the Australian Microscopy & Microanalysis Research Facility at the RMIT University. This research was undertaken in part on the soft X-ray beamline at the Australian Synchrotron, Victoria, Australia.

Supporting information for this article is available on the WWW under http://dx.doi.org/10.1002/anie.201209597.

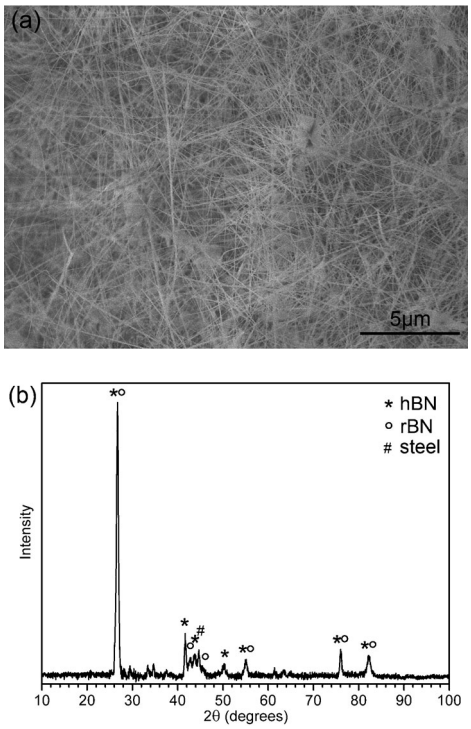

Figure 1. SEM image (a) and XRD pattern (b) of the product. The charging artefacts in the SEM image are due to the electrical insulation of the product.

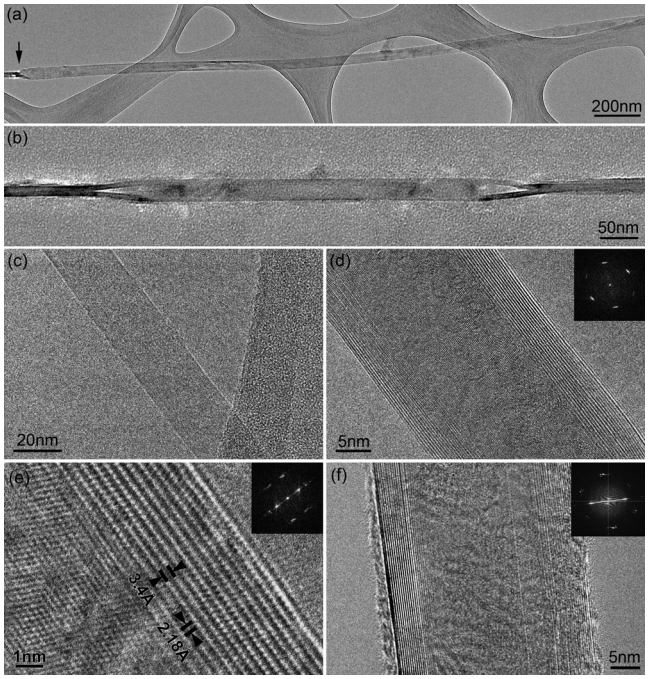

Figure 2. TEM images of a) a partially unzipped BNNR (the unzipping stop site is marked with an arrow); b) a partially unzipped BNNR with two unzipping stop sites; c)–f) two BNNRs at higher magnifications, with the FFTs inserted.

Some of the partially unzipped BNNRs have two or more unzipping stop sites, as shown in Figure 2b. This suggests that for these BNNRs, unzipping happens possibly after the formation of BNNTs rather than during BNNT growth, because it is unlikely that a BNNR can grow back to a BNNT if unzipping happens during BNNT growth. Some BNNRs have narrowed ends (see Figure S5 in the Supporting Information), which appears to be because they were unwrapped from BNNTs with flat caps. Figure 2c–e shows a BNNR with a width of 26 nm. The (002) lattice fringes with a spacing of 3.4 Å at the edges suggest that it has approximately 15 layers (5.1 nm thick) and very smooth edges. The appearance of the (002) lattice fringes indicates that the BNNR has curled edges. Such curled edges are commonly found in both GNRs and BNNRs obtained from nanotube unzipping.[6,10b,11] Possible causes are the different circumferences and curvatures of the inner and outer walls of the original multiwalled nanotubes, partial unzipping of nanotubes, and the reduction of the free surface and dangling bond energies at the edges. The fast Fourier transform (FFT) reveals that most of the BNNR exhibits a hexagonal pattern, while the two curled edges show the (00ℓ) spots. In the higher magnification TEM image in Figure 2e, the resolved lattice dots with an average distance of 2.18 Å in the edge region of the BNNR correspond to (10-10) lattice spacing in hBN and indicate that it has a well-defined stacking. According to the FFTs, this BNNR has an armchair orientation. Unlike carbon nanotubes (CNTs), which normally show no preferential helicity, BNNTs are more likely to have a uniform orientation in each tube,[8] and this also applies to BNNRs. Our studies show that the majority of the BNNRs and BNNTs are zigzag oriented (see Figure S6in the Supporting Information), consistent with previous studies.[6,8] Figure 2f shows a BNNR with zigzag orientation, as indicated by the inserted FFT. This BNNR also shows (002) lattice fringes at the two edges, indicating a width of 6.84 nm, corresponding to roughly 20 layers. The number of layers in the BNNRs depends on the number of walls in the unzipped nanotubes. Fewer-layer BNNRs as thin as double-layer can be produced by mild sonication of the thicker BNNRs (see Figures S2 and S3 in the Supporting Information).[10]

Since high-quality BNNRs are prerequisite for realizing the predicted properties and successful applications, we used NEXAFS spectroscopy to investigate the crystallinity and level of point defects or chemical impurities of the directly produced BNNRs. Figure 3a compares the NEXAFS spectrum of our product (containing both BNNRs and BNNTs) with that of an hBN single crystal[12] around the B K-edge region. Both samples show a strong and sharp π^* resonance at 192.0 eV and broad σ^* resonances above 197 eV, corresponding to core-level electron transitions to the unoccupied antibonding π^* and σ^* orbitals according to the dipole selection rule.[13] This suggests that the structures of BNNRs and BNNTs are similar to that of hBN. The broadening of the B π^* resonance can be used to elucidate the amount of disorder in the material. The full-widths at half-maximum (FWHMs) of the π^* resonance for our product and the single crystal are 325 and 322 meV, respectively. The very small difference indicates that our product has very high crystallinity, consistent with the TEM results (Figure 2e). Hexagonal BN materials tend to have O-decorated N vacancies[13b,14] which give rise to three satellite peaks at 192.6, 193.2, and

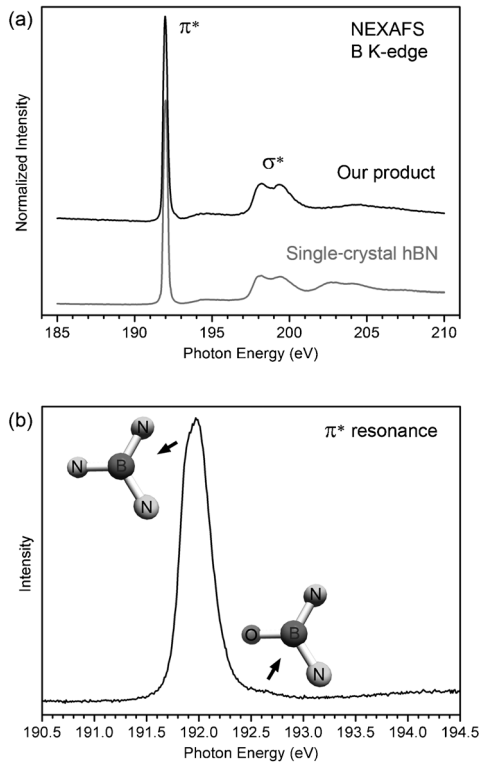

Figure 3. a) Comparison of NEXAFS spectra of our product (black) and an hBN single crystal (gray) around the B K-edge region; b) a high-resolution scan through the π* resonance of the product, showing only a very weak satellite peak at 192.6 eV representing one O atom occupying an N vacancy site in the planar ring.

193.9 eV in the B K-edge region, corresponding to one, two, and three nitrogen vacancies decorated by O atoms in a hexagonal ring. These three satellite peaks are often found in hBN materials, including BN particles,[14] BN thin films,[13c,15] BNNTs,[16] and BN nanosheets.[17] The hBN single crystal shows no obvious satellite peaks in the NEXAFS spectrum around the B K-edge region and therefore has few defects. Our product only shows a weak satellite peak at 192.6 eV (Figure 3b), indicating a low level of point defects mainly in the form of single vacancies (one O atom occupying one N vacancy). These O defects could be intrinsic to the BNNRs (O from impurities in the reaction gas during synthesis) or are introduced extrinsically after exposure to air (healing of N point defects or doping at the edges of the BNNRs).[14] The NEXAFS spectrum shows no detectable C or Li bonds, indicating few C and Li impurities in the product. The NEXAFS spectrum of the product around the N K-edge region can be found in Figure S7 in the Supporting Information. Overall, the BNNRs have high chemical purity and good crystallinity.

Earlier studies showed that Li strongly promotes the formation of hBN crystals[18] and high-quality BNNTs.[19] However, no unzipping of BNNTs has been reported before. We studied our intermediate products and found that all the Li_2O had reacted with the milled B to form lithium orthoborate (Li_3BO_3) at 800 °C (see Figure S8 in the Supporting Information). Li_3BO_3 is not stable at higher temperatures and decomposes to Li vapor and small BO/B_2O_2 clusters which are effective precursors for BNNT/BNNR formation in an NH_3 atmosphere.[19c] To determine the unzipping mechanism, we conducted three experiments: heating the as-grown BNNTs with 1) Li at 350 °C in Ar for 50 h; 2) Li_2O at 1200 °C in NH_3 for 3 h; and 3) Li at 1200 °C in NH_3 for 3 h. Although it has been reported that the heating of BNNTs with potassium (K) at an elevated temperature is able to unzip nanotubes, the heating of our BNNTs with Li in Ar at 350 °C for an extended period does not yield BNNRs (see Figure S9 in the Supporting Information), possibly because Li atoms alone are too small to expand the interplanar distance for unzipping to occur.[11,20] After the heating of BNNTs with Li_2O, some unzipping is observed and the unzipping seems to be caused by the etching of BNNTs by Li_2O (see Figure S10 in the Supporting Information). The best unzipping result is from the third experiment, that is, the heating of BNNTs with Li in NH_3, after which about half of BNNTs are unzipped (see Figure S11 in the Supporting Information). This establishes that Li plus NH_3 is the key for the high yield of BNNRs. As mentioned previously, Li alone is not effective for unzipping; however, Li–NH_3 species have been found to facilitate the expansion of the interplanar spacing and achieve unzipping.[20a] Therefore, we propose that during the synthesis process, Li–NH_3 species may penetrate into BNNTs on defect sites and the intercalation of the compounds expands the interplanar spacing so that the BN sp^2 bonds break. With the help of the strain in nanotubes,[10b] the bond breaking (unzipping) can extend along the BNNTs to form BNNRs, as evidenced by the smooth edges of our BNNRs. It is worth mentioning that in our method nanotubes are grown in an intercalating environment; the hollow interior and even the interplanar spacing of nanotubes could be filled with intercalating compounds, which makes unzipping occur more easily and during the nanotube growth process. The observed standard interlayer spacing of the BNNRs and the absence of Li may be a consequence of the instability of the intercalating compound at lower temperatures. The crystallinity of the BNNRs is high thanks to the presence of Li, as earlier studies have shown that Li strongly promotes formation of hBN,[18] and high-quality BNNTs have been successfully produced when Li is involved.[19] Li is a strong reducing agent that removes oxygen impurities in the BNNTs so that high chemical purity can be achieved, as shown by the NEXAFS results. The milling of B powder creates highly reactive B nanoparticles with an average particle size of 45 nm[9b,c] that enhance the reaction with Li_2O and increase the yield of BNNTs. When unmilled B powder is used, the yield of BNNTs/BNNRs in the crucible is much lower, as less Li_3BO_3 is formed and therefore fewer BO/B_2O_2 precursors and less Li is available for unzipping (see Figure S8 in the Supporting Information).

The fact that no unzipping was observed previously when Li_2O was used for BNNT synthesis may be because not enough Li was available for intercalation. We notice that BNNRs are produced only in the crucible where a high concentration of Li is around. When an alumina substrate was placed downstream of the crucible at a distance of about 2 cm in the direction of the gas flow, a high-purity BNNT film could

be produced on the substrate (because the small B clusters could be brought to the substrate by the gas flow to form BNNTs, similar to the chemical vapor deposition method described by Huang et al.[19c]); however, no unzipping is found on the substrate, despite the high proportion of BNNRs found in the crucible. The Li concentration at the downstream substrate is much lower due to dilution by the gas flow and may not be enough for unzipping. This is consistent with the experiment in which an excess of Li is heated with BNNTs in NH_3 at 1200 °C and a high yield of BNNRs results. In light of the proposed mechanism, higher ratios of Li_2O to milled B powder were tested for a possible higher unzipping ratio. However, the addition of too much Li_2O seems to be harmful to BNNT growth in the crucible (lower BNNT yield and therefore fewer BNNRs) and it was found that the Li_2O/B molar ratio should be no higher than 0.5:1.

Synchrotron vacuum ultraviolet (VUV) spectroscopy was used to investigate the optical properties of the BNNRs. Figure 4 shows the photoluminescence excitation (PLE)

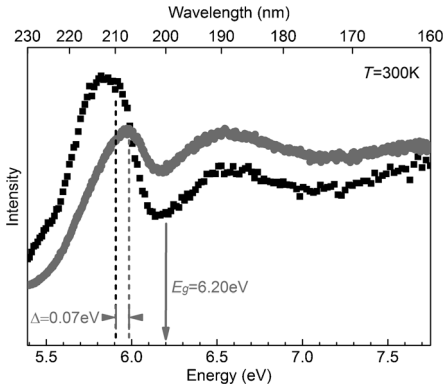

Figure 4. PLE spectra from a mixture of BNNRs and BNNTs (black) as well as BNNTs only (gray) at room temperature.

spectra from the mixture of BNNRs and BNNTs as well as BNNTs (without BNNRs). The BNNTs show an excitation peak at 5.98 eV (207.3 nm) which is followed by a plateau (around 6.17 eV) as well as an intensity increase from 6.20 eV (200.0 nm). Similar to the case of hBN,[21] the peak at 5.98 eV can be attributed to Frenkel excitons with lattice interaction, and the onset of the intensity increase at 6.20 eV can be assigned to free excitons following a bandgap excitation. So the estimated bandgap of the BNNTs is around 6.20 eV which is smaller than that of hBN.[21a] The sample containing BNNRs (ca. 40 %) has a similar bandgap value to BNNTs, but the excitation peak is located at lower energy 5.91 eV (209.8 nm), representing a redshift of 0.07 eV. The difference can be attributed to the different optical properties of BNNTs and BNNRs. That is, BNNRs have a larger exciton binding energy than BNNTs, possibly because of greater quantum confinement and therefore more localized excitons in BNNRs.[22] So BNNRs with even stronger excitonic effects than either hBN or BNNTs should have a better photoluminescence quantum yield and are intriguing optoelectronic nanomaterials.[23]

In summary, high-quality BNNRs have been produced by unzipping during nanotube synthesis. The BNNRs are normally several micrometers long and tens of nanometers wide. The BNNRs have smooth edges and uniform helicities. The thickness of the BNNRs depends on the wall number of the unzipped nanotubes and can be reduced to double-layer using a simple sonication treatment. NEXAFS investigations indicated that the BNNRs are of high chemical purity and crystallinity. The unzipping is likely to arise from the intercalation of BNNTs by Li–NH_3 species formed during the nanotube synthesis. It would be interesting to test whether the in situ unzipping concept is suitable for the large-scale production of high-quality GNRs.

Experimental Section

Amorphous B powder (96 %, Fluka) was first milled in anhydrous NH_3 gas at ca. 300 kPa using a vertical ball mill. The milling process lasted for 150 h at a speed of 110 rpm. The milled B powder was mixed with Li_2O powder at Li_2O/B molar ratios of 0.15:1 to 0.30:1. The mixed powder was placed at the bottom of an alumina crucible and heated to 1200 °C in NH_3 gas (changed from N_2 at 200 °C) at a flow rate of 0.2 L min^{-1} for 3 h.

Supra 55VP SEM, JEOL 2100F and 2100 TEM, and Panalytical XRD instruments were used to investigate the product. The NEXAFS analyses were performed in the ultrahigh-vacuum chamber (10^{-10} mbar) at the undulator soft X-ray spectroscopy beamline of the Australian Synchrotron, Victoria, Australia. Due to the insulating nature of BN material, a floodgun releasing 10 eV electrons was used to discharge the surface. The partial electron yield (PEY) signals were recorded using a hemispherical electron analyzer with nine channel electron multipliers (SPECS Phoibos 150). For the wide scans in B and N K-edge regions, 20 meV energy steps were used, and for the high-resolution scans around the B π* resonance, the step size was set to 10 meV. The NEXAFS data were normalized to the photoelectron current of the photon beam, measured on an Au grid. The hBN single crystal was synthesized by the high-pressure solvent method of Taniguchi et al.[12] The photoconductivity excitation was conducted at the high-flux cylindrical-grating monochromators (CGM) beamline BL03 A1 at the National Synchrotron Radiation Research Center (NSRRC), Taiwan. The emission receiving energy was set to 3.7 eV and the spectrum resolution was 0.3 nm.

Received: November 30, 2012
Published online: March 4, 2013

Keywords: boron nitride · nanoribbons · nanostructures · solid-phase synthesis

[1] C. H. Park, S. G. Louie, *Nano Lett.* **2008**, *8*, 2200 – 2203.
[2] W. Chen, Y. F. Li, G. T. Yu, C. Z. Li, S. B. B. Zhang, Z. Zhou, Z. F. Chen, *J. Am. Chem. Soc.* **2010**, *132*, 1699 – 1705.
[3] a) A. Lopez-Bezanilla, J. S. Huang, H. Terrones, B. G. Sumpter, *Nano Lett.* **2011**, *11*, 3267 – 3273; b) D. K. Samarakoon, X.-Q. Wang, *Appl. Phys. Lett.* **2012**, *100*, 103107; c) Z. H. Zhang, X. C. Zeng, W. L. Guo, *J. Am. Chem. Soc.* **2011**, *133*, 14831 – 14838; d) F. W. Zheng, G. Zhou, Z. R. Liu, J. Wu, W. H. Duan, B. L. Gu, S. B. Zhang, *Phys. Rev. B* **2008**, *78*, 205415.
[4] A. J. Du, S. C. Smith, G. Q. Lu, *Chem. Phys. Lett.* **2007**, *447*, 181 – 186.
[5] H. Zeng, C. Zhi, Z. Zhang, X. Wei, X. Wang, W. Guo, Y. Bando, D. Golberg, *Nano Lett.* **2010**, *10*, 5049 – 5055.

[6] K. J. Erickson, A. L. Gibb, A. Sinitskii, M. Rousseas, N. Alem, J. M. Tour, A. K. Zettl, *Nano Lett.* **2011**, *11*, 3221 – 3226.
[7] L. Chen, Y. Hernandez, X. L. Feng, K. Mullen, *Angew. Chem.* **2012**, *124*, 7758 – 7773; *Angew. Chem. Int. Ed.* **2012**, *51*, 7640 – 7654.
[8] D. Golberg, Y. Bando, C. C. Tang, C. Y. Zhi, *Adv. Mater.* **2007**, *19*, 2413 – 2432.
[9] a) Y. Chen, L. T. Chadderton, J. FitzGerald, J. S. Williams, *Appl. Phys. Lett.* **1999**, *74*, 2960 – 2962; b) L. H. Li, Y. Chen, A. M. Glushenkov, *Nanotechnology* **2010**, *21*, 105601; c) L. H. Li, Y. Chen, A. M. Glushenkov, *J. Mater. Chem.* **2010**, *20*, 9679 – 9683.
[10] a) Y. Hernandez, V. Nicolosi, M. Lotya, F. M. Blighe, Z. Y. Sun, S. De, I. T. McGovern, B. Holland, M. Byrne, Y. K. Gun'ko, J. J. Boland, P. Niraj, G. Duesberg, S. Krishnamurthy, R. Goodhue, J. Hutchison, V. Scardaci, A. C. Ferrari, J. N. Coleman, *Nat. Nanotechnol.* **2008**, *3*, 563 – 568; b) L. Jiao, X. Wang, G. Diankov, H. Wang, H. Dai, *Nat. Nanotechnol.* **2010**, *5*, 321 – 325.
[11] D. V. Kosynkin, W. Lu, A. Sinitskii, G. Pera, Z. Sun, J. M. Tour, *ACS Nano* **2011**, *5*, 968 – 974.
[12] T. Taniguchi, K. Watanabe, *J. Cryst. Growth* **2007**, *303*, 525 – 529.
[13] a) J. Barth, C. Kunz, T. M. Zimkina, *Solid State Commun.* **1980**, *36*, 453 – 456; b) M. Petravic, R. Peter, I. Kavre, L. H. Li, Y. Chen, L. J. Fan, Y. W. Yang, *Phys. Chem. Chem. Phys.* **2010**, *12*, 15349 – 15353; c) L. H. Li, M. Petravic, B. C. C. Cowie, T. Xing, R. Peter, Y. Chen, C. Si, W. Duan, *Appl. Phys. Lett.* **2012**, *101*, 191604.
[14] I. Caretti, I. Jimenez, *J. Appl. Phys.* **2011**, *110*, 023511.
[15] M. Niibe, K. Miyamoto, T. Mitamura, K. Mochiji, *J. Vac. Sci. Technol. A* **2010**, *28*, 1157 – 1160.
[16] L. Li, L. H. Li, Y. Chen, X. Dai, T. Xing, M. Petravic, X. Liu, *Nanoscale Res. Lett.* **2012**, *7*, 417.
[17] L. H. Li, Y. Chen, G. Behan, H. Zhang, M. Petravic, A. M. Glushenkov, *J. Mater. Chem.* **2011**, *21*, 11862 – 11866.
[18] a) T. S. Bartnitskaya, A. V. Kurdyumov, V. I. Lyashenko, N. F. Ostrovskaya, I. G. Rogovaya, *Powder Metall. Met. Ceram.* **1996**, *35*, 296 – 300; b) Y. L. Gu, M. T. Zheng, Y. L. Liu, Z. L. Xu, *J. Am. Ceram. Soc.* **2007**, *90*, 1589 – 1591.
[19] a) M. Terauchi, M. Tanaka, H. Matsuda, M. Takeda, K. Kimura, *J. Electron Microsc.* **1997**, *46*, 75 – 78; b) H. Yang, B. Yoshio, T. Chengchun, Z. Chunyi, T. Takeshi, D. Benjamin, S. Takashi, G. Dmitri, *Nanotechnology* **2009**, *20*, 085705; c) Y. Huang, J. Lin, C. C. Tang, Y. Bando, C. Y. Zhi, T. Y. Zhai, B. Dierre, T. Sekiguchi, D. Golberg, *Nanotechnology* **2011**, *22*, 145602; d) M. Terauchi, M. Tanaka, K. Suzuki, A. Ogino, K. Kimura, *Chem. Phys. Lett.* **2000**, *324*, 359 – 364.
[20] a) A. G. Cano-Márquez, F. J. Rodríguez-Macías, J. Campos-Delgado, C. G. Espinosa-González, F. Tristán-López, D. Ramírez-González, D. A. Cullen, D. J. Smith, M. Terrones, Y. I. Vega-Cantú, *Nano Lett.* **2009**, *9*, 1527 – 1533; b) G. Maurin, F. Henn, B. Simon, J. F. Colomer, J. B. Nagy, *Nano Lett.* **2001**, *1*, 75 – 79.
[21] a) L. Museur, G. Brasse, A. Pierret, S. Maine, B. Attal-Tretout, F. Ducastelle, A. Loiseau, J. Barjon, K. Watanabe, T. Taniguchi, A. Kanaev, *Phys. Status Solidi RRL* **2011**, *5*, 214 – 216; b) K. Watanabe, T. Taniguchi, *Phys. Rev. B* **2009**, *79*, 193104.
[22] S. D. Wang, Q. Chen, J. L. Wang, *Appl. Phys. Lett.* **2011**, *99*, 063114.
[23] a) L. H. Li, Y. Chen, M. Y. Lin, A. M. Glushenkov, B. M. Cheng, J. Yu, *Appl. Phys. Lett.* **2010**, *97*, 141104; b) L. H. Li, Y. Chen, B.-M. Cheng, M.-Y. Lin, S.-L. Chou, Y.-C. Peng, *Appl. Phys. Lett.* **2012**, *100*, 261108.

